PCCP

PAPER

View Article Online
View Journal | View Issue

Cite this: *Phys. Chem. Chem. Phys.*, 2025, **27**, 8377

Matrix-isolation IR spectra of iodotrifluoroethylene (C_2F_3I)†

Malte Feßner, [ab] Julien Bloino [ab] and Christian Merten *[ab]

The infrared spectra of iodotrifluoroethylene (ITFE) recorded under matrix-isolation (MI) conditions in *para*-hydrogen, neon and argon were investigated. The experimental spectra were analyzed by comparison with computed anharmonic spectra obtained in the second-order vibrational perturbation theory (VPT2) framework at the MP2 and revDSD-PBEP86-D3BJ levels of theory. In *para*-hydrogen and neon matrices, the experimentally observable bands in the range of 1800–650 cm^{-1} could be assigned to vibrational transitions of monomeric ITFE. The spectral resolution even allowed assignments of transitions arising from ^{13}C-isotopologues and the observation of various higher-order resonances in the range up to ~3550 cm^{-1}. A comprehensive series of MI experiments in argon obtained by varying several experimental parameters revealed a dependence of the spectra on the deposition temperature. The spectra generally showed strong site-splitting effects due to the existence of different local environments around the ITFE molecule. Detailed analysis of the experimental spectra resulted in the identification of bands which are differently affected by matrix annealing. This observation led to the conclusion that ITFE occupies two major matrix sites of different stability. Calculations on ITFE dimers confirmed that spectral changes during annealing are due to the formation of dimers, which are stabilized through π–π interactions.

Received 22nd January 2025,
Accepted 23rd March 2025

DOI: 10.1039/d5cp00292c

rsc.li/pccp

Introduction

Halogen bonding (XB) interactions[1–6] are currently considered as alternative to classical Coulomb and hydrogen bonding interactions in various areas of chemistry. While applications typically make use of large electron-deficient molecules to increase the XB strength, it is more convenient to select neutral XB complexes of small donor and acceptor molecules as model systems for fundamental studies on XB interactions. Their reduced size makes easier the application of accurate theoretical models, while their lack of conformational dynamics and relatively simple electronic structure facilitate theoretical analyses. From an experimental perspective, the characterization of such weak intermolecular interactions in the solution phase is often challenging as they inevitably compete with solute–solvent interactions. Furthermore, IR spectroscopic signatures of complexes may sometimes only slightly deviate from those of the corresponding monomers, and hence will not be resolvable in broad solution phase spectra.

Gas-phase spectroscopies and methods taking advantage of inert environments are thus the methods of choice for the characterization of such complexes. Rotational spectroscopy, for instance, has been utilized to gain insights into lone-pair (lp)···π interactions in complexes of C_2F_3Cl with water[7] and ammonia[8] or for C_2H_4···ClF,[9] to name a few examples. Using liquid rare gases as solvents,[10] Herrebout and co-workers investigated weakly bound complexes, among others,[11,12] of CF_3X (X = Cl, Br, I or H) with ethene and propene[13] in liquid argon (LAr) and with benzene and toluene in liquid krypton (LKr) at 150 K.[14] They also investigated C_2F_3X···$N(CD_3)_3$ (with X = F, Cl, Br, I) as model systems with potentially competing lp···π and halogen bonding interactions.[15]

The matrix isolation (MI) technique[16,17] involves the trapping of weakly bound clusters in solid rare gas matrices, that are prepared by spraying mixtures of the target compounds and the host gas onto a cryogenic window, which is typically held at temperatures markedly below the melting point of the host gas. This procedure traps mostly complexes that are already formed in the gas phase. Through diffusion processes, that are initiated either due to excess thermal energy of the gas mixture during cooldown or by slightly warming the matrix after deposition, further complexation takes place. Due to the rigidity of the environment, large structural rearrangements are effectively suppressed, so that it is often possible to also trap thermodynamically less favourable clusters.[18,19] Through MI-IR

[a] *Ruhr-Universität Bochum, Fakultät für Chemie und Biochemie, Organische Chemie II, Universitätsstraße 150, 44801 Bochum, Germany. E-mail: christian.merten@ruhr-uni-bochum.de; Web: https://www.mertenlab.de*
[b] *Scuola Normale Superiore, Piazza dei Cavalieri 7, 56126 Pisa, Italy*

† Electronic supplementary information (ESI) available: Additional spectra plots, experimental spectra and computational data from VPT2 analysis. See DOI: https://doi.org/10.1039/d5cp00292c

spectroscopy, C–Cl···π interactions between CCl_4 and ethene[20] (Ar and N_2 matrix), as well as the complexes of CCl_4 or CBr_4 with acetone[21] could be characterized, for instance.[22–25]

In a recent MI-IR study,[26] we characterized complexes of iodotrifluoroethylene C_2F_3I (ITFE), the title compound of the present study, with *N*,*N*-dimethyl ferrocenyl amine. While the amine-derivative expectedly showed C–I···N interactions with ITFE, we also observed spectral signatures indicative of C–I···π halogen bonding and π···π interactions. The latter interactions could also be identified in MI-IR spectra of ITFE with the parent ferrocene. We also briefly characterized ITFE itself and discussed the spectral signatures of the monomer and some dimeric species. However, when studying complexes of ITFE with other XB-acceptors, we realized that the MI-IR spectra of pure ITFE were more complicated than we initially thought. In fact, we found a strong dependence of the spectra on the host gas and deposition temperature. In the present study, we thus further refine our picture of the structure of ITFE in cryogenic matrices (*para*-hydrogen, Ne, Ar) and revise earlier band assignments.

Results and discussion

ITFE possesses 12 fundamental vibrational transitions, of which five are predicted to occur in the spectral range above 600 cm^{-1}, which is experimentally accessible to us. According to harmonic calculations,[15,26,27] the observable fundamentals are the C=C stretching mode ($\nu_{C=C}$, 1770–1750 cm^{-1}), the out-of-phase C–F stretching in =CFF ($\nu_{CF2,oop}$, 1350–1300 cm^{-1}), the C–F stretching of =CFI (ν_{C-F}, 1200–1150 cm^{-1}), and in-phase stretching of C–F in =CFF ($\nu_{CF2,ip}$, out-of-phase coupled to C–I stretching, around 1000 cm^{-1}). At ~650 cm^{-1}, a fifth, very weak fundamental mode is predicted to arise from an in-plane bending motion of the entire molecule (ν_δ).

Experimental matrix-IR spectra of ITFE were recorded in *para*-hydrogen (pH_2) and neon matrices deposited at 4 K, and in argon matrices prepared at various temperatures between 4 and 25 K. Upon inspection of the spectra (*cf.* Fig. 1), differences in band positions can be observed between the matrix host gases. Such matrix-induced band shifts are not unusual and arise from differences in the polarizabilities of the media as well as from packing effects.[28,29] It is furthermore important to note that there are clearly more strong bands visible than the five fundamental transitions expected in this spectral range. In the C=C stretching range, one sharp band can be identified in the spectra recorded for pH_2 and Ne, while there is at least one additional band visible in the Ar matrix. In fact, depending on the deposition temperature, up to five bands can be identified (see discussion below). In the spectral range where $\nu_{CF2,oop}$ lies, there are at least four bands identifiable in pH_2, while even more weak features are found in the Ar matrix. Similar observations can be made in the other two highlighted spectral ranges.

To assign as many of the experimentally observed features as possible, we carried out spectral calculations at various levels of theory. In the following, we will first discuss the computational results in comparison to the spectra of ITFE recorded in pH_2 and Ne, before subsequently moving to the spectra recorded in argon.

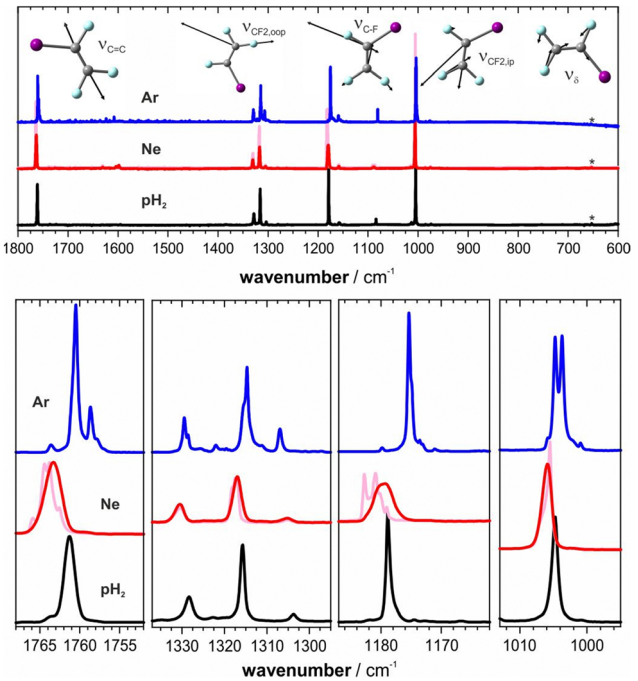

Fig. 1 Experimental IR spectra of ITFE recorded under different matrix-isolation conditions (pH_2 : 4 K, 1 : 1000; Ne : 4 K, 1 : 1800, two different depositions; Ar : 15 K, 1 : 1800). Top: Overview spectra and the displacement vectors corresponding to the five fundamental modes present in the experimentally accessible range. Bottom: Expanded views on the experimental spectra around the four strong fundamental transitions.

Band assignments in pH_2 and Ne matrices

To identify the most suitable theoretical basis for the computation of the IR spectrum of ITFE, we first carried out calculations at the hybrid-DFT level using B3LYP[30–32] in its dispersion corrected variant (D3BJ),[33] at double-hybrid DFT levels with the B2PLYP-D3BJ[34] and the revDSD-PBEP86-D3BJ[35] functionals, and lastly using pure MP2.[36–39] A triple-ζ basis set (def2TZVP[40]) was used for all calculations. As expected, the different levels of electronic structure theory gave different band positions in the harmonic approximation (*cf.* Fig. S1, ESI†). In line with previous observations,[26,27,41] the B3LYP-D3BJ functional provided a good match for the three strong vibrational modes, that involve stretching motions of C–F bonds ($\nu_{CF2,oop}$, ν_{C-F}, $\nu_{CF2,ip}$), even without application of a frequency scaling factor, while the energy of the C=C stretching mode was overestimated. After applying suitable uniform scaling factors, however, the spectrum computed at the MP2 level generally matched exceptionally well all four strong experimental band positions. In the order revDSD-PBEP86-D3BJ, B2PLYP-D3BJ, B3LYP-D3BJ, the other three methods led to increasingly strong deviations from the experimental band positions.

As noted above, the experimental spectra show additional intense bands that are not associated with fundamental

transitions (*cf.* Fig. 1, overview). In a study on halogen-bonding of ITFE in LKr,[15] Herrebout *et al.* assigned some of them to combinations and overtones. However, due to the sharp bandwidth of the pH_2-matrix measurement, significantly more bands could be resolved than in LKr. Hence, to complete the assignments, we computed the IR spectrum of ITFE including anharmonicity by means of second-order vibrational perturbation theory (VPT2) at all four computational levels.[42–47] To our delight, the resulting IR spectrum obtained at either the MP2 or revDSD-PBEP86-D3BJ level reproduced many of the very small features that were missing in the harmonic spectrum (*cf.* Fig. 2 and Fig. S1 (ESI†) show the results for the other methods as well). Interestingly, revDSD-PBEP86-D3BJ in fact performed notably better than MP2 and almost perfectly matched many experimental band positions and relative intensities. It must be stressed that no frequency scaling factor was applied on top of the VPT2 energies.

The most noteworthy band assignment is probably that of the very intense band at 1328 cm^{-1}, which is a combination mode of the fundamentals 7 and 4. Yet, the VPT2 calculation on ITFE could not explain all small bands and distinct bands, such as those present at 1736 or 1723 cm^{-1}, remained unexplained. As Herrebout *et al.* assigned one of them to a ^{13}C-isotopologue,[15] we computed the anharmonic spectra of ITFE with ^{13}C at either position of the C=C bond. This allowed us to confirm the assignment of these two bands as the C=C stretching vibrations of the ^{13}CFI and ^{13}CFF isotopologues and to make further assignments for bands in the fingerprint region of the pH_2-spectra (*cf.* colour-coded band assignments in Fig. 2 and Table 1). Notably, the anharmonic calculations even correctly predict minute energy shifts between vibrational states of different isotopologues (*cf.* ESI† for further discussions).

It should be mentioned that ITFE possesses many more combination modes and overtones than those highlighted in the fingerprint region. Likewise, it must be acknowledged that the VPT2 calculations nicely reproduce these spectral features over a wide range (*cf.* Fig. S3, ESI†). The spectral intensities and computed spectra even allow the identification of the overtone of the C=C stretching mode. The fundamental occurs at 1764 cm^{-1}, while its overtone is experimentally found at 3524 cm^{-1}.

Comparing the spectrum recorded for the Ne matrix with the pH_2 matrix reveals differences for only two peaks, the C=C stretching mode and C–F stretching of =CFI. Both appear highly structured, an indication of site splitting effects.[48] Annealing of the Ne matrix at 9 K, a temperature at which the matrix is very close to evaporation, changed the band shapes only marginally, further stressing that this mode may be particularly prone to matrix site effects. We noticed that minor

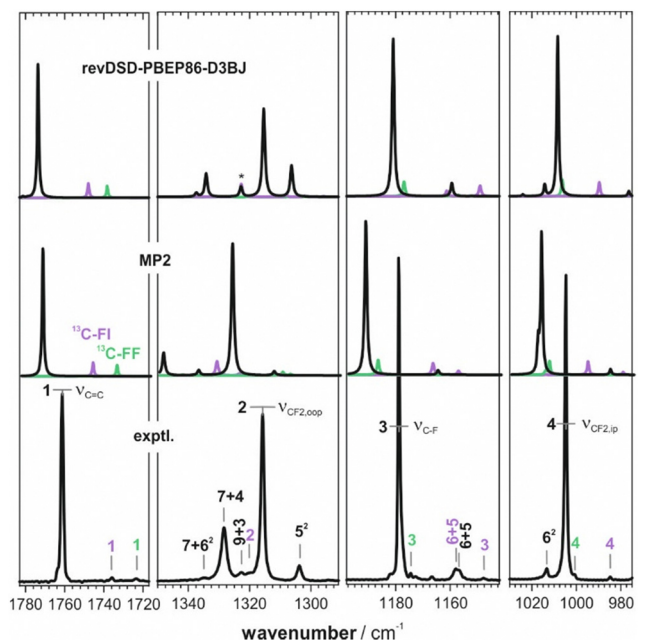

Fig. 2 Experimental spectra of ITFE in a pH_2 matrix deposited at 4 K compared to the computed anharmonic (VPT2) spectra obtained at the MP2 and revDSD-PBEP86-D3BJ levels of theory. Band labels refer to the excited modes and quanta (superscripts), when higher than 1. Colour-coded band assignments refer to ^{13}C-isotopologues. Band broadening was simulated with Lorentzian functions and 0.5 cm^{-1} half-width at half-height. Instead of scaling the intensities of ^{13}C-isotopologues to the actual natural abundancy of +1%, they were scaled to 10% for clarity. (*Fundamental 2 of ^{13}C–FI and combination mode 9 + 3 overlap. For analysis and discussion see ESI.†)

Table 1 Band assignments for the fingerprint region of the IR spectrum of ITFE recorded in a pH_2 matrix based on VPT2 calculations on the isolated monomer (M) and its ^{13}C-isotopologues (^{13}C-FI and ^{13}C-FF) at the revDSD-PBEP86-D3BJ level of theory. The full set of computational data including predicted intensities is provided in the ESI

ν_{exp}/cm^{-1}	ν_{VPT2}/cm^{-1}	Assignment	Origin
652.8	654.5	5	M
906.6	913.3	11 + 10	M
939.1	943.9	8 + 1	M
974.2	976.4	7 + 5	M
984.8	989.7	4 ($\nu_{CF2,ip}$)	^{13}C-FI
1000.9	1006.3	4 ($\nu_{CF2,ip}$)	^{13}C-F_2
1004.5	1008.4	4 ($\nu_{CF2,ip}$)	M
1013.3	1014.2	6^2	M
1083.0	1126.7	10^2	M[a]
1147.7	1149.9	3 (ν_{C-F})	^{13}C-FI
1153.2	1157.0	6 + 5	^{13}C-FF
1156.6	1159.4	6 + 5	M
1158.0	1161.3	6 + 5	^{13}C-FI
1174.5	1177.0	3 (ν_{C-F})	^{13}C-FF
1178.9	1180.9	3 (ν_{C-F})	M
1279.8	1276.2	2 ($\nu_{CF2,oop}$)	^{13}C-FF
1294.3	1295.9	9 + 3	^{13}C-FI
1303.8	1306.3	5^2	M
1315.8	1315.4	2 ($\nu_{CF2,oop}$)	M
1319.5	1322.7	2 ($\nu_{CF2,oop}$)	^{13}C-FI
1322.7	1322.8	9 + 1	M
1328.3	1334.2	7 + 4	M
1334.8	1337.4	7 + 6^2	M
1686.2	1685.1	6 + 3	M
1723.5	1738.3	1 ($\nu_{C=C}$)	^{13}C-FF
1735.9	1747.9	1 ($\nu_{C=C}$)	^{13}C-FI
1761.3	1773.6	1 ($\nu_{C=C}$)	M
1831.0	1832.0	5 + 3	M

[a] Assignment supported by Geboes *et al.*[15]

traces of water in the matrix led to a collapse of the site splitting (*cf.* Fig. S4, ESI†),[49] so that matrix isolation studies on interactions of ITFE with other molecules in neon will most likely not show such strong splitting effects.

Band assignments for ITFE in an Ar matrix

All bands observed in the experimental spectra in pH_2 and Ne matrices can be assigned to monomeric ITFE. As noted above, in the context of a halogen bonding study, we have previously investigated the IR spectrum of ITFE in an Ar matrix and noted that the spectrum showed many additional bands not obviously assignable to the monomer. We thus concluded that a prominent band at 1758.7 cm^{-1} adjacent to the C═C stretching band at 1760.4 cm^{-1} would arise from dimeric species.

For the present study, we have re-investigated the spectra of ITFE in an Ar matrix and carried out a comprehensive series of experiments, varying the concentration (*i.e.*, the mixing ratio ITFE:Ar), the flow rate (*i.e.*, deposition rates that determine the quality of the growth of the matrix), and the deposition temperature (*i.e.*, the softness of the matrix during deposition). Interestingly, for a given deposition temperature, no differences were observed for concentrations ranging from 1 : 900 to 1 : 3600 or by varying the flow rate (*cf.* Fig. 3a). Only the variation of the deposition temperature changed the spectral patterns. To our surprise, the aforementioned band at 1758.7 cm^{-1} occurred in all spectra and it showed approximately the same relative intensity (1 : 3) compared to the C═C stretching band at 1760.4 cm^{-1} independent of the experimental parameters. In fact, a variation of the deposition temperature generated several additional bands (*e.g.*, at 1763.6 and 1757.8 cm^{-1}), while the bands at 1760.4 and 1758.7 cm^{-1} remained in a stable relative intensity ratio. Changes in the range around $\nu_{CF2,oop}$ (fundamental "2") were weak and as this range was congested with contributions from several combination modes and overtones, it was not further considered in the analysis. The spectral signatures around ν_{C-F} and $\nu_{CF2,ip}$, *i.e.* the fundamentals "3" and "4", however, were found to differ notably depending on the deposition temperature, with the intensity ratio between the bands at 1004.7 and 1003.6 cm^{-1} showing the most prominent changes.

After annealing of the matrices at 35 K (*cf.* Fig. 3b), the C═C stretching regions of the spectra taken at 10 K and higher converged to very similar band-shapes. New bands consistently occurred at 1763.6, 1757.8, 1757.2 and 1756.4 cm^{-1}. The band at 1760.4 cm^{-1} generally decreased, but the band at 1758.7 cm^{-1} remained surprisingly constant in intensity. No other band was found to be equally robust upon annealing. On the contrary, around ν_{C-F}, new bands occurred at 1175.3 and 1174.0 cm^{-1}, with the latter showing an interesting trend in intensity. The band pattern around $\nu_{CF2,ip}$ remained rather stable, but a slight change in relative intensity could nonetheless be noted.

Site-splitting is commonly observed for the Ar-matrix,[28,29,50,51] especially of small molecules. Several matrix-isolation studies have reported the existence of multiple matrix sites in Argon with different stabilities. For both carbon dioxide[52] and dimethyl sulfate,[53] for instance, two matrix sites are observed of which one is significantly more stable than the other. Given the discussed dependencies of the spectral patterns of ITFE in an Ar matrix on temperature and the changes upon annealing, we propose that monomeric ITFE resides in two major matrix sites of different stability. Accordingly, we interpret the bands at 1760.4 and 1758.7 cm^{-1} as C═C stretching modes of ITFE molecules sitting in matrix pockets of different stability. It is remarkable, however, that the lower-energy band remains basically unaffected by annealing attempts, indicating a particularly high stability. For the other spectral regions, such direct assignments are more difficult, not least because of overlaps with combination states and overtones, and the occurrence of small site-splitting effects. Bands increasing in intensity during annealing should subsequently be considered the preferred dimeric species.

To assist in the assignment of further bands, we computed the IR spectra of ITFE dimers. To this end, geometry optimizations and IR spectra calculations were carried out on several dimer structures. Common to all low-energy dimers was the fact that they are stabilized by π–π interactions (*cf.* Fig. 4). Hence, they differed solely by the relative orientation of the molecules and molecular planes. The two lowest-energy structures (c1 and c2 in Fig. 4) are basically iso-energetic and thus

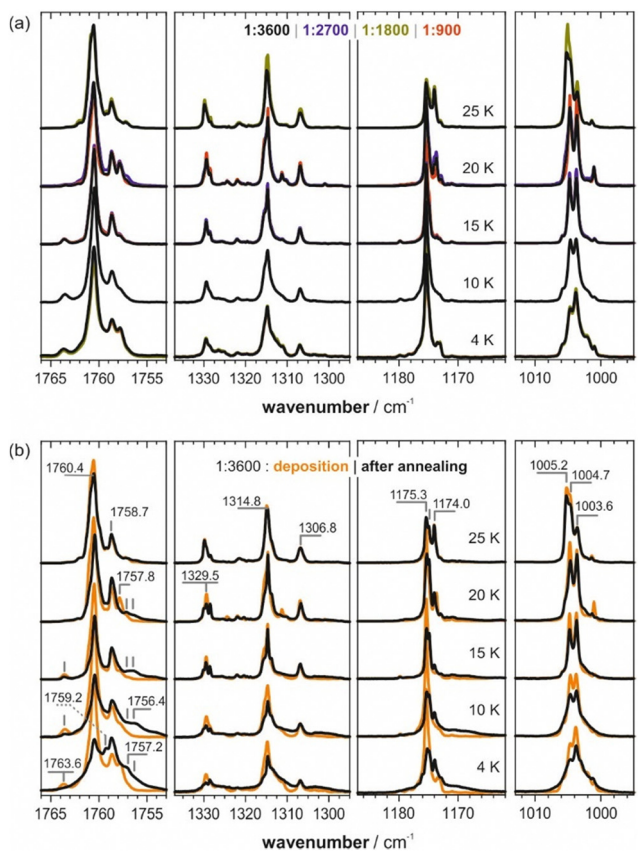

Fig. 3 (a) Experimental spectra of ITFE in an Ar matrix deposited at different temperatures and concentrations. The corresponding difference spectra are shown in Fig. S4 (ESI†). (b) Spectra of ITFE/Ar = 1 : 3600 after annealing at 35 K with band markers for the signatures discussed in the text.

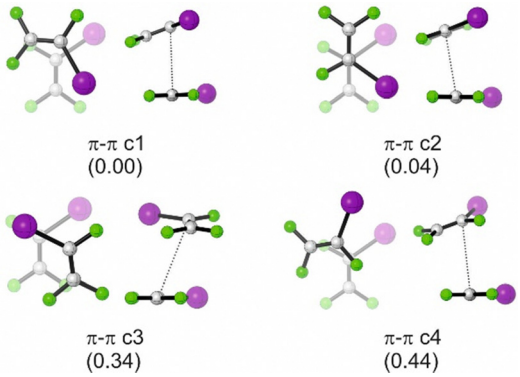

Fig. 4 The four lowest-energy dimeric structures of ITFE considered in the analysis of the experimental matrix-IR spectra. Relative energies (in kcal mol^{-1}) obtained from single-point calculations at the DLPNO-CCSD(T) level of theory[54,55] on the revDSD-PBEP86-D3BJ optimized structures are given between parentheses.

equally likely to form during deposition and even more upon annealing. Other possible dimer geometries, involving C–I···π or C–I···I interactions, were found to be notably higher and thus were not considered in the analysis (*cf.* Fig. S8 and Table S1, ESI†).

Each of the four lowest-energy dimers has characteristic spectral band shapes, which are independent of the level of theory and whether a harmonic or anharmonic approach was used (*cf.* Fig. S6, ESI† and Fig. 5, respectively). However, comparing the band positions relative to those of the ITFE monomer, they are found to differ significantly between computational levels. For instance, at the MP2 level, the two bands related to the C=C stretching modes of each structure are consistently found at lower wavenumbers than the monomer. With revDSD-PBEP86-D3BJ, one of the two bands is predicted to be blue-shifted with respect to the monomer and the other one is red-shifted. At the anharmonic level, more contradicting

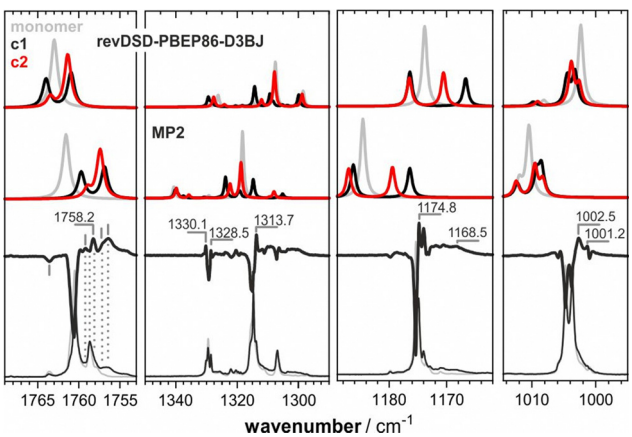

Fig. 5 Comparison of the experimental spectra of ITFE/Ar recorded at 15 K with the computed anharmonic spectra obtained at the revDSD-PBEP86-D3BJ and MP2 levels of theory within the VPT2 framework. Band markers in the difference spectra refer to bands arising during annealing, which are associated with dimeric species of ITFE. Note that the frequency axis was scaled by 0.994 to fit the bands into the spectral ranges.

predictions of the relative band positions were observed. For instance, with revDSD-PBEP86-D3BJ, the fundamental of mode 4 of the monomer ($\nu_{CF2,ip}$, 1010–1000 cm^{-1}) is at lower energy compared to those of the dimers, while the anharmonic MP2 calculations place it at higher energies. Hence, in addition to the need to consider that the monomer occupied two different matrix sites, the comparison between the experimental and computed spectra was further complicated by uncertainties in the computed band positions.

For this reason, we focussed our comparison of computed and experimental spectra on the data recorded for the 15 K deposition and especially on the difference spectrum (*cf.* Fig. 5). The latter spectrum amplifies spectral signatures of species generated and depleted during annealing. Bands of the lowest-energy dimers should occur as positive features, while negative bands are associated with higher-energy dimers and monomeric ITFE disappearing during annealing. In doing so, the new features in the C=C stretching region, *i.e.*, the bands at 1759.2 and 1757.2 cm^{-1}, could be reasonably well explained with the predicted two bands of dimers, which supports an assignment of the π–π c1 and π–π c2 to the bands at 1758.2/1756.5 and 1757.2 cm^{-1}. Considering the predicted relative order of bands obtained from revDSD-PBEP86-D3BJ, the disappearing band at 1763.6 cm^{-1} may be assigned to the π–π c3 dimer (*cf.* Fig. S7 for an overview of all computed anharmonic spectra, ESI†). The growth of the broad features around 1170 cm^{-1} may also arise from the two lowest-energy dimers, but the new sharp bands cannot be assigned to any of the four dimer species. Likewise, the new features adjacent to $\nu_{CF2,ip}$ around 1002 cm^{-1} also agree well with the predicted band shapes of the two lowest-energy dimers. While the spectral calculations confirm that the spectra of ITFE in Ar matrices show mostly heavily site-split bands of the monomeric species, it must be concluded that the experimental and computational data do not allow for an unambiguous correlation of spectral features to specific dimeric species.

Conclusions

In the present study, we investigated the IR spectra of ITFE recorded under matrix-isolation conditions in various host gases. The experimental spectra were analysed by means of anharmonic spectral calculations at the VPT2 level using different electronic structure calculation methods. For pH$_2$ and Ne matrices, the experimental spectra matched very well computations on the ITFE monomer, and most experimentally observable bands could be assigned to fundamentals, combinations and overtones, or arising from the presence of ^{13}C-isotopologues. This comparison stressed the need to go beyond harmonic spectral calculations to fully assign vibrational signatures, and simultaneously showcased the performance of the VPT2 approach to accurately account for resonances. In the case of argon matrices, additional bands were observed directly after deposition, and annealing resulted in significant spectral changes. A series of MI-experiments with

varying deposition conditions allowed us to identify two matrix sites for the ITFE monomer, of which one was significantly more stable. It persisted during annealing, while ITFE in the less stable site formed dimers. Based on the computed spectra, only very few bands related to dimer species could be univocally assigned to the two lowest-energy structures (*cf.* Fig. 4). Spectral calculations also revealed that the exact shift of the C═C stretching bands in dimer structures depended strongly on the chosen level of theory, which can be problematic for the precise assignment of such a highly sought band. In this context, the weak performance of a commonly used method such as MP2 was particularly unexpected, as it consistently underestimated the energies of the complexes' bands.

Our study led to two main conclusions for future studies on intermolecular interactions of ITFE. First, despite the very limited possibilities to anneal the matrix and thus to form larger amounts of intermolecularly bound clusters after deposition, pH_2 and Ne are more suited as host gases than Ar. The bands arising from the additional argon matrix site bear the risk of overlapping with signatures of other complexes and cause unnecessary convolution of the spectra. Secondly, one should not rely solely on computed spectra from MP2 as the shifts of the C═C stretching band caused by intermolecular interactions may be predicted incorrectly. As the performances of B3LYP-D3BJ, B2PLYP-D3BJ and revDSD-PBEP86-D3BJ were similar in terms of relative positions of the most sensitive C═C stretching bands, either of them should suffice to analyse the changes occurring in that spectral region.

Experimental details

Materials

ITFE was purchased from ABCR GmbH, Germany, in 97% purity and used without further purification. Gases were obtained from air liquide: H_2 in 99.9999% purity, Ne in 99.999% purity and Ar in 99.999% purity.

Matrix isolation IR spectroscopy

Experiments were carried out using either an APD Cryogenics DE-204SL for operation down to 10 K or a Janis SHI-4R cryostat operating down to 4 K. Ar depositions were carried out on both systems to ensure that spectral signatures are not instrument-dependent. *para*-Hydrogen (>99%) was generated using a home-built converter based on a Janis CCS-100/2004 cryostat.[56] Sample mixtures were prepared in a standard gas manifold and sprayed onto a BaF_2 window using a calibrated flow controller (MKS). Annealing of Ar matrices was done by slowly heating the window to 35 K, holding it at this temperature for 25 minutes, followed by a cooldown to the initial temperature. IR spectra were recorded at 0.2 cm^{-1} resolution using a Bruker INVENIO-R FT-IR spectrometer, accumulating 50 scans.

Computational details

Geometry optimizations and IR spectra calculations were carried out at various levels of theory in the gas phase using Gaussian 16.[57] Starting structures for the optimizations were generated manually, considering all possible relative orientations of the monomer species allowing for π···π, C–I···π, C–I···F and other interactions. Anharmonic calculations at the VPT2 level were carried out by first generating the necessary constants by numerical differentiation along mass-weighted normal coordinates, as implemented in Gaussian 16, with a constant step of 0.01 $\mu^{1/2}$ Å. Resonances in VPT2 were identified following the protocol described in ref. 58 with the same numerical thresholds. Removed terms were then reintroduced variationally and the final energies obtained by diagonalization of the generated polyads. A locally modified version of Gaussian was used for all VPT2 calculations. Spectra were simulated from the computed dipole strengths by assigning a Lorentzian band shape of 0.5 cm^{-1} half-width at half-height. Frequencies of the harmonic spectra were uniformly scaled as mentioned in the text. Single-point energies at the DLPNO-CCSD(T) level of theory were computed with ORCA 6.[59–61] Structures were rendered using CylView.[62]

Data availability

The data supporting this article have been included as part of the ESI.†

Conflicts of interest

There are no conflicts to declare.

Acknowledgements

This work was funded by the Deutsche Forschungsgemeinschaft (DFG, German Research Foundation) under Germany's Excellence Strategy (EXC-2033, project number 390677874), through the Research Training Group "Confinement Controlled Chemistry" (GRK 2376, project number 331085229), the DFG's Heisenberg program (ME 4267/5-1; project no. 418661145), and a research grant (ME 4267/6-1; project no. 418662566), by the Boehringer Ingelheim Foundation through a Plus-3 grant, and by the Italian Ministry of University of Research (PRIN grant num. 2020HTSXMA).

References

1 R. L. Sutar, E. Engelage, R. Stoll and S. M. Huber, *Angew. Chem., Int. Ed.*, 2020, **59**, 6806–6810.
2 G. Cavallo, P. Metrangolo, R. Milani, T. Pilati, A. Priimagi, G. Resnati and G. Terraneo, *Chem. Rev.*, 2016, **116**, 2478–2601.
3 L. C. Gilday, S. W. Robinson, T. A. Barendt, M. J. Langton, B. R. Mullaney and P. D. Beer, *Chem. Rev.*, 2015, **115**, 7118–7195.

4 S. H. Jungbauer, S. M. Walter, S. Schindler, L. Rout, F. Kniep and S. M. Huber, *Chem. Commun.*, 2014, **50**, 6281–6284.
5 S. M. Huber, J. D. Scanlon, E. Jimenez-Izal, J. M. Ugalde and I. Infante, *Phys. Chem. Chem. Phys.*, 2013, **15**, 10350–10357.
6 E. Corradi, S. V. Meille, M. T. Messina, P. Metrangolo and G. Resnati, *Angew. Chem., Int. Ed.*, 2000, **39**, 1782–1786.
7 Q. Gou, G. Feng, L. Evangelisti and W. Caminati, *Angew. Chem., Int. Ed.*, 2013, **52**, 11888–11891.
8 Q. Gou, L. Spada, Y. Geboes, W. A. Herrebout, S. Melandri and W. Caminati, *Phys. Chem. Chem. Phys.*, 2015, **17**, 7694–7698.
9 H. I. Bloemink, J. H. Holloway and A. C. Legon, *Chem. Phys. Lett.*, 1996, **250**, 567–575.
10 W. Herrebout, in *Halogen Bonding I - Impact on Materials Chemistry and Life Sciences*, ed. P. Metrangolo and G. Resnati, Springer International Publishing, 2015.
11 D. Hauchecorne, A. Moiana, B. J. van der Veken and W. A. Herrebout, *Phys. Chem. Chem. Phys.*, 2011, **13**, 10204–10213.
12 B. Michielsen, J. J. J. Dom, B. J. van der Veken, S. Hesse, M. A. Suhm and W. A. Herrebout, *Phys. Chem. Chem. Phys.*, 2012, **14**, 6469–6478.
13 D. Hauchecorne, N. Nagels, B. J. van der Veken and W. A. Herrebout, *Phys. Chem. Chem. Phys.*, 2012, **14**, 681–690.
14 N. Nagels, D. Hauchecorne and W. A. Herrebout, *Molecules*, 2013, **18**, 6829–6851.
15 Y. Geboes, F. De Proft and W. A. Herrebout, *J. Phys. Chem. A*, 2015, **119**, 5597–5606.
16 I. R. Dunkin, *Chem. Soc. Rev.*, 1980, **9**, 1–23.
17 V. E. Bondybey, A. M. Smith and J. Agreiter, *Chem. Rev.*, 1996, **96**, 2113–2134.
18 C. Merten and Y. Xu, *Chem. Phys. Chem.*, 2013, **14**, 213–219.
19 C. Merten and Y. Xu, *Angew. Chem., Int. Ed.*, 2013, **52**, 2073–2076.
20 N. Ramanathan, K. Sundararajan, K. Vidya and E. D. Jemmis, *Spectrochim. Acta, Part A*, 2016, **157**, 69–78.
21 P. Banerjee and I. Bhattacharya, *Spectrochim. Acta, Part A*, 2021, **250**, 119355.
22 D. Pal, S. K. Agrawal, A. Chakraborty and S. Chakraborty, *Phys. Chem. Chem. Phys.*, 2020, **22**, 22465–22476.
23 D. Pal, A. Chakraborty and S. Chakraborty, *Chem. Phys.*, 2022, **555**, 111451.
24 B. Suryaprasad, S. Chandra, N. Ramanathan and K. Sundararajan, *J. Mol. Struct.*, 2021, **1224**, 129288.
25 P. Wang, N. Zhao and Y. Tang, *J. Phys. Chem. A*, 2017, **121**, 5045–5055.
26 N. M. Kreienborg, F. Otte, C. Strohmann and C. Merten, *Phys. Chem. Chem. Phys.*, 2023, **25**, 15110–15114.
27 N. M. Kreienborg and C. Merten, *Phys. Chem. Chem. Phys.*, 2019, **21**, 3506–3511.
28 A. J. Barnes and H. E. Hallam, *Q. Rev., Chem. Soc.*, 1969, **23**, 392–409.
29 A. J. Barnes and W. J. Orville-Thomas, *FT-IR Matrix Isolation Studies*, Dordrecht, 1980.
30 A. D. Becke, *J. Chem. Phys.*, 1993, **98**, 5648–5652.
31 C. Lee, W. Yang and R. G. Parr, *Phys. Rev. B: Condens. Matter Mater. Phys.*, 1988, **37**, 785–789.
32 P. J. Stephens, F. J. Devlin, C. F. Chabalowski and M. J. Frisch, *J. Phys. Chem.*, 1994, **98**, 11623–11627.
33 S. Grimme, S. Ehrlich and L. Goerigk, *J. Comput. Chem.*, 2011, **32**, 1456–1465.
34 S. Grimme, *J. Chem. Phys.*, 2006, **124**, 034108.
35 G. Santra, N. Sylvetsky and J. M. L. Martin, *J. Phys. Chem. A*, 2019, **123**, 5129–5143.
36 K. Raghavachari, G. W. Trucks, J. A. Pople and M. Head-Gordon, *Chem. Phys. Lett.*, 1989, **157**, 479–483.
37 M. Head-Gordon, J. A. Pople and M. J. Frisch, *Chem. Phys. Lett.*, 1988, **153**, 503–506.
38 M. J. Frisch, M. Head-Gordon and J. A. Pople, *Chem. Phys. Lett.*, 1990, **166**, 275–280.
39 M. Head-Gordon and T. Head-Gordon, *Chem. Phys. Lett.*, 1994, **220**, 122–128.
40 F. Weigend and R. Ahlrichs, *Phys. Chem. Chem. Phys.*, 2005, **7**, 3297–3305.
41 N. M. Kreienborg and C. Merten, *Chem. – Eur. J.*, 2018, **24**, 17948–17954.
42 C. Merten, J. Bloino, V. Barone and Y. Xu, *J. Phys. Chem. Lett.*, 2013, **4**, 3424–3428.
43 J. Bloino, M. Biczysko and V. Barone, *J. Phys. Chem. A*, 2015, **119**, 11862–11874.
44 J. Bloino, A. Baiardi and M. Biczysko, *Int. J. Quantum Chem.*, 2016, **116**, 1543–1574.
45 Q. Yang, M. Mendolicchio, V. Barone and J. Bloino, *Front. Astron. Space Sci.*, 2021, **8**, 665232.
46 M. Fusè, G. Longhi, G. Mazzeo, S. Stranges, F. Leonelli, G. Aquila, E. Bodo, B. Brunetti, C. Bicchi, C. Cagliero, J. Bloino and S. Abbate, *J. Phys. Chem. A*, 2022, **126**, 6719–6733.
47 N. M. Kreienborg, Q. Yang, C. H. Pollok, J. Bloino and C. Merten, *Phys. Chem. Chem. Phys.*, 2023, **25**, 3343–3353.
48 S. Ostwald, M. A. Suhm and S. Coussan, *Phys. Chem. Chem. Phys.*, 2019, **21**, 1277–1284.
49 D. Forney, M. E. Jacox and W. E. Thompson, *J. Mol. Spectrosc.*, 1993, **157**, 479–493.
50 J. Nieminen, J. Murto and M. Räsänen, *Spectrochim. Acta, Part A*, 1991, **47**, 1495–1504.
51 I. D. Reva, S. G. Stepanian, L. Adamowicz and R. Fausto, *J. Phys. Chem. A*, 2001, **105**, 4773–4780.
52 D. F. Dinu, M. Podewitz, H. Grothe, T. Loerting and K. R. Liedl, *Phys. Chem. Chem. Phys.*, 2020, **22**, 17932–17947.
53 A. Borba, A. Gómez-Zavaglia, P. N. N. L. Simões and R. Fausto, *Spectrochim. Acta, Part A*, 2005, **61**, 1461–1470.
54 C. Riplinger and F. Neese, *J. Chem. Phys.*, 2013, **138**, 034106.
55 C. Riplinger, B. Sandhoefer, A. Hansen and F. Neese, *J. Chem. Phys.*, 2013, **139**, 134101.
56 L. Andrews and X. Wang, *Rev. Sci. Instrum.*, 2004, **75**, 3039–3044.
57 M. J. Frisch, G. W. Trucks, H. B. Schlegel, G. E. Scuseria, M. A. Robb, J. R. Cheeseman, G. Scalmani, V. Barone, G. A. Petersson, H. Nakatsuji, X. Li, M. Caricato, A. V. Marenich, J. Bloino, B. G. Janesko, R. Gomperts,

B. Mennucci, H. P. Hratchian, J. V. Ortiz, A. F. Izmaylov, J. L. Sonnenberg, F. Ding, F. Lipparini, F. Egidi, J. Goings, B. Peng, A. Petrone, T. Henderson, D. Ranasinghe, V. G. Zakrzewski, J. Gao, N. Rega, G. Zheng, W. Liang, M. Hada, M. Ehara, K. Toyota, R. Fukuda, J. Hasegawa, M. Ishida, T. Nakajima, Y. Honda, O. Kitao, H. Nakai, T. Vreven, K. Throssell, J. A. Montgomery Jr., J. E. Peralta, F. Ogliaro, M. J. Bearpark, J. J. Heyd, E. N. Brothers, K. N. Kudin, V. N. Staroverov, T. A. Keith, R. Kobayashi, J. Normand, K. Raghavachari, A. P. Rendell, J. C. Burant, S. S. Iyengar, J. Tomasi, M. Cossi, J. M. Millam, M. Klene, C. Adamo, R. Cammi, J. W. Ochterski, R. L. Martin, K. Morokuma, O. Farkas, J. B. Foresman and D. J. Fox, *Gaussian 16 Rev. C.01*, Wallingford, CT, 2016.

58 Q. Yang and J. Bloino, *J. Phys. Chem. A*, 2022, **126**, 9276–9302.

59 F. Neese, *Wiley Interdiscip. Rev.: Comput. Mol. Sci.*, 2022, **12**, e1606.

60 F. Neese, *Wiley Interdiscip. Rev.: Comput. Mol. Sci.*, 2012, **2**, 73–78.

61 F. Neese, F. Wennmohs, U. Becker and C. Riplinger, *J. Chem. Phys.*, 2020, **152**, 224108.

62 C. Y. Legault, *CYLview 1.0b*, Université de Sherbrooke, 2009.

